

Power Electronic Circuits for Magnetic Energy Harvesters

Jinyeong Moon, Steven B. Leeb

Department of Electrical Engineering and Computer Science
Massachusetts Institute of Technology
Cambridge, MA 02139, USA

Abstract—Compared to many other energy harvesting schemes, harvesting energy from magnetic fields offers potential advantages for energy extraction and sensing. A magnetic energy harvester provides great flexibility for sensors and monitoring applications for condition-based monitoring of electromagnetic actuators, including vibration and thermal monitoring. A core must be managed or operated with carefully timed saturation to ensure maximum power extraction, a complex problem given the nonlinear saturation characteristics of a magnetic core [1]. This paper presents a simulator-friendly “circuit model” for a magnetic core, and uses this model to design and demonstrate several power electronic circuit solutions for harvesting energy. The circuit model has an excellent accuracy to represent the core regardless of the level of saturation, and the proposed design techniques are shown by simulation and analytical results that they substantially boost the amount of power harvest.

Index Terms—Magnetic, Energy, Power, Harvester, Saturation, Flux, Shaping, Capacitor, Transfer, Window, Alignment, FSC, TWA, Current-driven, Rectifier

I. INTRODUCTION

Energy available to a sensor or monitoring hardware may be limited in situations where the sensor is only powered by an environmental energy harvester [2], [3], [4], [5]. Available energy and power from the harvester may profoundly limit sample rate, data precision, signal processing, transmission bandwidth, and data storage capacity and rates [6]. The selection of environmental parameter from which to harvest energy (e.g., vibration [7], [8], [9], [10], thermal gradients [11], [12], light [13], etc.) can limit the performance and even the possibility of a power-harvesting sensor node. This paper considers the design of magnetic field energy harvesters and associated power electronic circuits. These circuits are used to create a sensor node called VAMPIRE (vibration assessment monitoring point with integrated recovery of energy) for measuring *in-situ* vibration, temperature, and other environmental parameters for motors [2]. The design techniques and power harvesting circuits presented in this paper could be applied to many other sensing and actuation problems.

This approach uses a magnetic core configured similarly to a traditional current-sense transformer. A line powering a load of interest passes through the center of the core. A relatively high-turns secondary winding is used for recovering energy for a monitoring circuit. This paper presents three new circuit designs to enhance the amount of extracted energy: the flux-shaping capacitor (FSC) method, the transfer window

alignment (TWA) method, and an active rectifier. An important analytical concept for designing these harvesters is the “transfer window,” explained in the next section. The proposed rectifier is to reduce the switching loss, caused by nonideal diodes in a rectifier. To validate and verify the design of energy harvester circuits using any of these methods, it is convenient to have an analytical model of the highly nonlinear magnetic core. This paper therefore begins with the development of a “circuit-friendly” core model based on the analytical model presented in [1]. The model will be shown to have excellent predictive power, and will be used to design and evaluate demonstrations of the harvesting techniques.

II. BACKGROUND

The analysis in [1] involves two load types: resistive loads and constant voltage loads. The resistive load model is simple and illustrative of core behaviors, but not appropriate for a magnetic energy harvester, especially when the load is a DC-DC converter or a supercapacitor powering a sensor suite. We will use the resistive load model where appropriate to illustrate techniques, but the “constant voltage” load will be used to design and evaluate the behavior of circuits.

The core in the magnetic energy harvester is energized by a primary winding that is effectively driven by a current source. The insertion impedance of the harvester transformer is generally low, that is, the load under observation sets or commands the current flowing through the primary of the harvester. Saturation of the harvester core is determined by the interaction of this primary current with the time and level of voltage applied to the secondary winding of the harvester.

When a magnetic core is saturated, the secondary side voltage across the core becomes essentially zero, because the time derivative of the magnetic flux density in the core (B) is near zero in saturation. The magnetizing inductance (referred to the secondary side) is therefore extremely low during this period, and little power is coupled from the primary winding. With a high permeability core, when the core is not saturated, the magnetizing inductance is relatively high, and significant power transfer can occur to the secondary. The “transfer window” is introduced in [1] to describe this distinct region when significant power flow occurs through the core across the transformer. We develop circuit design methods based on this concept of the transfer window in order to permit control and maximization of harvested energy.

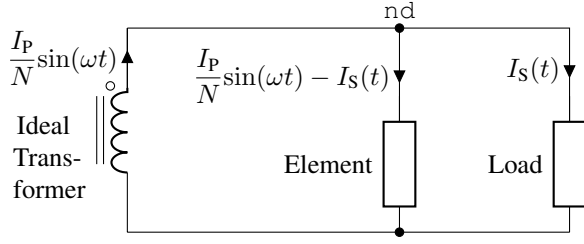


Fig. 1. Circuit representation of the circuit model

III. CIRCUIT MODEL

The Maxwell model discussed in [1] is complete for simulating a circuit if all the components are described in a numerical solver. The model provides little intuitive insight, and requires a custom-designed numerical solver that quickly becomes undesirable when combined with the behavior of a proposed power electronic circuit on the secondary that consists of switching devices. Here, we develop a model for a magnetically saturating core that can be directly employed in SPICE. This model will be used to validate experimental results for our power harvester converters.

A. Circuit Model

We denote a number of windings of the secondary, the saturation flux density, outer radius, inner radius, and height of a toroidal core by N , A_{CORE} , B_{SAT} , r_{OD} , r_{ID} , and h , respectively. The flux linkage in the toroidal core of the magnetic energy harvester can be described as:

$$\Lambda(t) = N \cdot h \cdot \int_{r_{\text{ID}}}^{r_{\text{OD}}} B(r, t) dr \quad (1)$$

Here, we approximate the spatial integration by modeling the core flux density at every radius as equal to the core flux density at $r_{\text{mid}} = (r_{\text{OD}} + r_{\text{ID}})/2$. Then, using the same saturation function as in [1], the expression for the flux can be approximated as:

$$\Lambda(t) \approx B_{\text{SAT}} (r_{\text{OD}} - r_{\text{ID}}) h N \times \frac{2}{\pi} \arctan \left(\frac{I_{\text{P}} \sin(\omega t) - N \cdot I_{\text{S}}(t)}{2 \pi r_{\text{mid}} \alpha} \right) \quad (2)$$

This equation can be written compactly as:

$$\Lambda(t) = \Lambda_{\text{MAX}} \cdot \frac{2}{\pi} \arctan \left(\frac{N}{\beta} I_{\mu}(t) \right) \quad (3)$$

using the parameters defined below:

$$\Lambda_{\text{MAX}} = B_{\text{SAT}} (r_{\text{OD}} - r_{\text{ID}}) h N = B_{\text{SAT}} A_{\text{CORE}} N \quad (4)$$

$$\beta = 2 \pi r_{\text{mid}} \alpha = l_{\text{FLUX}} \alpha \quad (5)$$

$$I_{\mu}(t) = \frac{I_{\text{P}}}{N} \sin(\omega t) - I_{\text{S}}(t) \quad (6)$$

By interpreting (6) as a KCL constraint, we can draw a node with three branches as illustrated in Fig. 1. The first branch is $I_{\text{P}}/N \cdot \sin(\omega t)$, supplying the current into the node. This is easily represented by an ideal current transformer with the

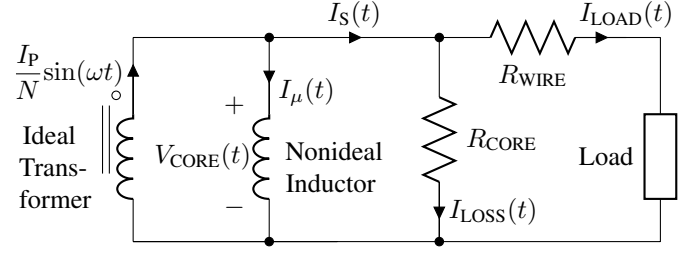


Fig. 2. Circuit model

winding ratio of $1 : N$ and primary current of $I_{\text{P}} \sin(\omega t)$. The second branch is $I_{\text{S}}(t)$, taking the current out of the node. It can be treated as a load current. The third branch is the current remainder, $I_{\mu}(t)$, as we defined. The equation (3) describes the relationship between current and flux of the element in the third branch, and we can further develop the relationship between voltage and current by time differentiation of the flux:

$$V_{\text{CORE}}(t) = \frac{\partial}{\partial t} \left[\Lambda_{\text{MAX}} \cdot \frac{2}{\pi} \arctan \left(\frac{N}{\beta} I_{\mu}(t) \right) \right] \quad (7)$$

The derivative of $\arctan(x)$ is $1/(1+x^2)$, resulting in a flux relationship in the general form of an inductor. The inductance is nonlinear and time-varying in an application with an ac current in the primary winding. This is consistent with intuition about the core, as, for an unsaturated core with constant permeability, we would expect the core to appear from winding terminals as an inductance.

Summarizing branch descriptions, we can present the circuit configuration as shown in Fig. 2. The circuit model builds from an ideal transformer and adds a nonideal inductor in parallel with it, while the Maxwell method has a lumped nonideal transformer that includes the effects of both. Using either a nonideal inductor element that supports a flux description, or a behavioral voltage element, the equation (7) can be directly used in SPICE with ease. The circuit model is attractive because it is easier to mix with power electronic components such as MOSFETs and diodes in SPICE. A concern remains in determining core loss, which affects the overall performance of the harvester. A SPICE simulation can track the voltage across and current through the nonideal magnetizing inductance and use these waveforms to calculate the area under a B-H curve as a scaled ratio of the maximum loss presented by the full hysteresis curve for the materials:

$$P_{\text{LOSS}} = P_{\text{LOSS-MAX}} \cdot \frac{I_{\text{PEAK}}}{I_{\text{SAT}}} \cdot \frac{B_{\text{PEAK}}}{B_{\text{SAT}}} \quad (8)$$

as described in [1]. A circuit simulator can therefore also accurately model core loss by updating the value of R_{CORE} with a numerical estimate. Additional loss mechanisms like conduction loss can also be modeled, e.g., by R_{WIRE} , as shown in Fig. 2.

In the following sections, we will verify the accuracy of the circuit model, and introduce circuit design techniques for a magnetic energy harvester based on this circuit model.

TABLE I
CORE PARAMETERS

B_{SAT}	1.190 T
$P_{LOSS-MAX}$	0.125 mW
α	2.2
β	0.142
Outer Radius (r_{OD})	12.25 mm
Inner Radius (r_{ID})	8.25 mm
Height (h)	9 mm
Flux Area (A_{CORE})	$3.6 \times 10^{-5} \text{ m}^2$
Flux Length (l_{FLUX})	$6.44 \times 10^{-2} \text{ m}$

B. Model Accuracy

The accuracy of this circuit model can be verified by comparison to experimental data and to a full Maxwell model of the core as described in [1]. Assuming the same core, Vacuumschmelze (VAC) VITROPERM 500F W380, the estimated parameter values, B_{SAT} , $P_{LOSS-MAX}$, α , β , and dimensional properties of the core are listed in Table I.

In Fig. 3, four plots are presented to compare the accuracy of the circuit model to the Maxwell model and the experiment. Model accuracy is considered with two load types, a resistive load and a constant voltage load. We tested with different I_P and N configurations. As illustrated in the figure, regardless of the load type, I_P , and N , the circuit model is as accurate as the Maxwell model, closely tracking the experiment. Approximations made in the modeling, e.g., uniformity of the magnetic flux density throughout the core and approximating the saturation characteristic with an arctan function provide excellent accuracy for designing energy harvesting systems.

IV. MAXIMIZING THE POWER HARVEST

The duration and level of the voltage applied to the secondary winding by the harvester circuitry determines when the flux in the core will build to saturation levels. At a high level, maximizing the power harvest boils down to the problem of keeping the core out of saturation for a “best” period of time. This window or period of time would ideally allow the fixed secondary current to flow for the longest period of time with the highest secondary voltage. This time period when current flows through the transformer action (while the core is not fully saturated) is the transfer window. Of course, the core could always be operated so that it never saturates. Figure 3 demonstrates that the unsaturated core, which is in a strictly linear region in lower R_{LOAD} or V_{LOAD} , always corresponds to a less-than-maximal power harvest. Permitting the core to eventually saturate over the course of a primary waveform cycle provides maximum power transfer. The trick is to time this saturation to maximize the energy extraction.

Three different circuit techniques can be used to maximize the extent and precise timing of the power transfer window. The first involves placing a capacitance in series with the core before a rectifier stage. The capacitor shapes the flux developed across the core, and lengthens the transfer window. The second is to connect the load to the core such that the middle of the transfer window is aligned with the peak of the

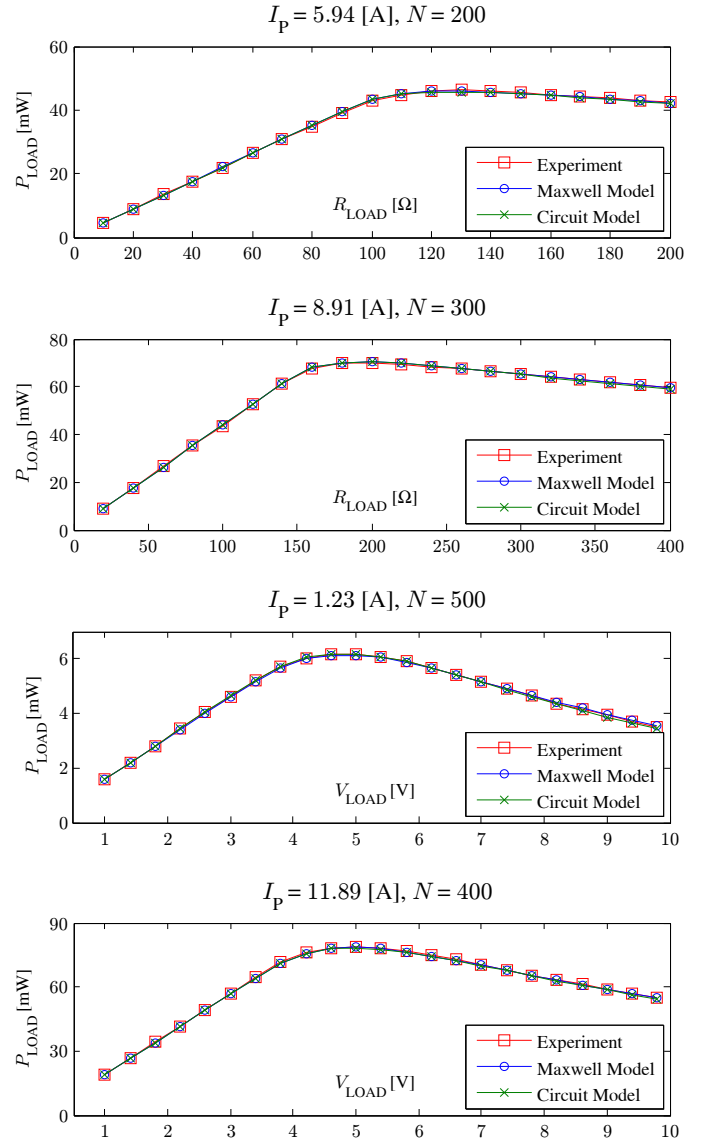


Fig. 3. Experimental verification of the circuit model

transformer current. At other times, the load is disconnected from the core, and the core is externally shorted to prevent itself from accumulating flux. The two techniques cannot be used at the same time; however each technique is capable substantially enhancing the power harvest compared to an unmodified current transformer. The third technique is to use a rectifier with active gate control instead of passive rectifiers. If the gate control is available at relatively low cost, e.g., from a microcontroller already serving in the sensor system, active rectification can be used with either one of the first two techniques.

A. Flux-shaping Capacitor (FSC)

Since the magnetizing inductor is not an ideal inductor, the load receives power only when the core is not saturated. This means that the transfer window is active when the magnetizing inductance appears as a large shunt impedance across the secondary. To lengthen the transfer window, we seek to reduce

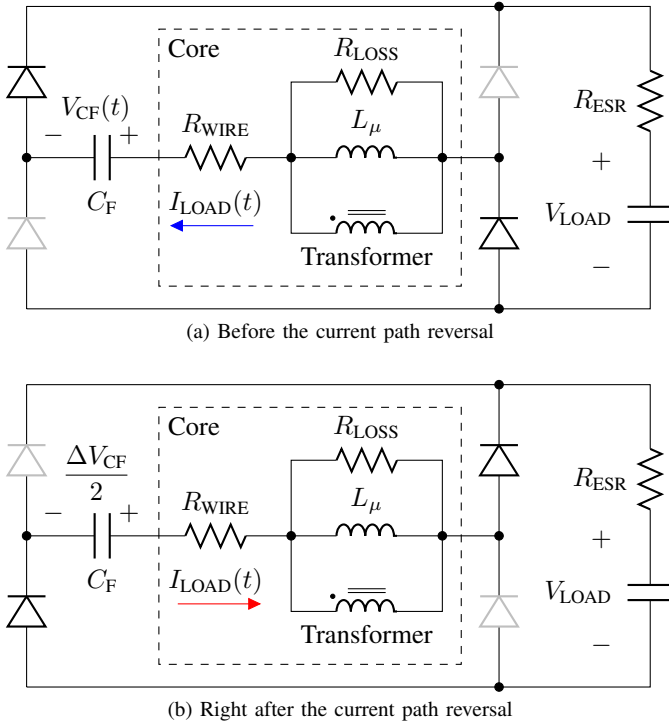


Fig. 4. The circuit example with flux-shaping capacitor

the volt-seconds applied to this inductor. The volt-seconds applied to the magnetizing inductance can be reduced by placing a capacitor C_F in series with the load. This capacitor charges during any particular half cycle. During the next half-cycle, the capacitor is charged with a voltage polarity opposite to that of the constant voltage load. The net voltage applied to the magnetizing inductance is therefore reduced, lengthening the power transfer window and increasing the power delivered to the load.

When C_F is added to the circuitry, we can no longer obtain a simple expression for the maximum power harvest point, as presented in (19) of [1]. Instead of finding an analytical solution, we develop an insight by analyzing the core behavior in a qualitative way. In Fig. 4(a), where the current flows to the left, the current charges up the flux-shaping capacitor, increasing $V_{CF}(t)$ until the core is saturated. When the core is saturated, the voltage across the magnetizing inductance becomes zero, preventing the transformer current from going into the load. At this instant, depending on the voltage across C_F , the diodes may either all turn-off or briefly switch to the alternate conduction path. If $V_{CF}(t)$ is higher than V_{LOAD} , then the current path briefly switches and supplies current from C_F into the load until $V_{CF}(t)$ is equal to V_{LOAD} , at which point the diodes turn off. This brief period continues power delivery to the load. If $V_{CF}(t)$ is not higher than V_{LOAD} , the diodes are all disconnected, keeping $V_{CF}(t)$ constant until the core recovers from the saturation and reverses the current direction. In the steady-state, net charge into the flux-shaping capacitor is zero. Therefore, both positive and negative peaks will have the same magnitude of $\Delta V_{CF}/2$.

Right after the reversal of the main current path, as illustrated in Fig. 4(b), the voltage across the core starts from

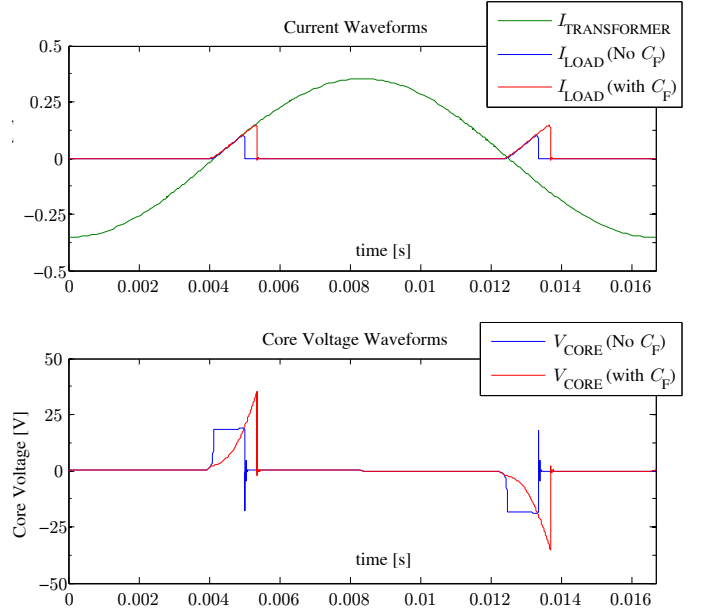


Fig. 5. Flux-shaping capacitor simulation example in hard saturation

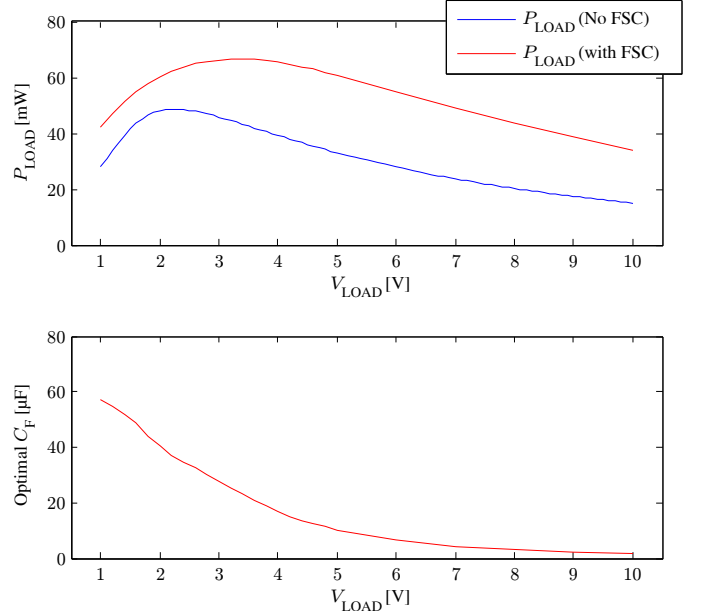


Fig. 6. Simulation of the flux-shaping capacitor method

$V_{LOAD} - \Delta V_{CF}/2$, whereas it is always V_{LOAD} if we do not use a flux-shaping capacitor. For a sinusoidal primary current, $V_{CF}(t)$ is a cosine wave, and, therefore, $V_{LOAD} - V_{CF}(t)$ becomes convex. This indicates that the transfer window is lengthened in the tail due to the flux shaping action of the capacitor. Lengthening the transfer window by a small amount can result in a great boost in power harvest. Figure 5 illustrates a simulation example, where the transfer window is visibly lengthened by a flux-shaping capacitor. To illustrate the effect, Fig. 5 shows simulated results with an operating point of $I_P = 50 A_{RMS}$, $N = 200$, $V_{LOAD} = 18 V$, and $C_F = 2.9 \mu F$. The power harvest is increased by 107.12% compared to the case with no flux-shaping capacitor.

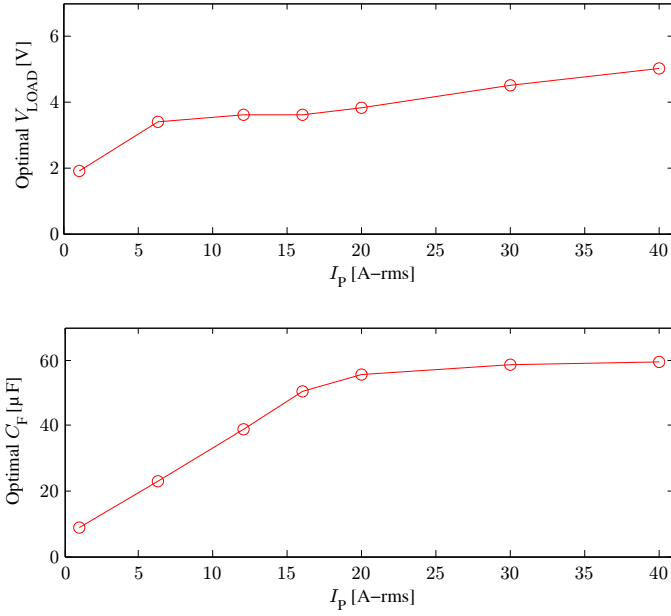


Fig. 7. Simulation of optimal V_{LOAD} and C_F vs. I_P , with $N = 200$

In a real design, we need to first find the optimal V_{LOAD} and C_F subject to given I_P and N configuration. Since it is not analytically possible to predict the peak, we swept both parameters to find the maximum power harvest as in Fig. 6. The lower plot represents the corresponding C_F that yields the maximum power harvest for each V_{LOAD} . In this example, we used $I_P = 6.27 A_{RMS}$, $N = 200$, and nonideal diodes for the rectifier, which has a diode voltage drop of 0.19 V. The maximum harvestable power of 48.6 mW without the flux-shaping capacitor now reaches 66.6 mW, which is a net increase of 37.04%. However, there is a major issue in this method that if the RMS of the primary current continuously changes, for example, in case of periodic motor speed control, optimal V_{LOAD} and C_F for the maximum power harvest also continuously change, as illustrated in Fig. 7. We used $N = 200$ for this figure. Changing V_{LOAD} can be accomplished by connecting a power converter with programmable duty cycle control as a load.

Two concerns associated with changing capacitance remain. First, the optimal capacitance spans a wide range as illustrated in Fig. 7. Second, an attempt to tune the capacitance, e.g., by selecting a capacitor from a bank of choices, requires a circuit that can effectively operate with the capacitor in a “floating” position in the circuit, complicating switch implementation.

If the primary current is extremely low such that the core never saturates during operation, adding a capacitor in series with the core, which maintains constant inductance in this case, can be viewed as a power factor corrector. This makes the waveform of the load current more rectangular, and results in higher average current. Due to this effect, the amount of power harvest is boosted even in the nonsaturated region with the flux-shaping capacitor, as shown near the initial linear region in Fig. 6. Since the load is a constant voltage source, the average power harvest is directly proportional to the average current, not the RMS current.

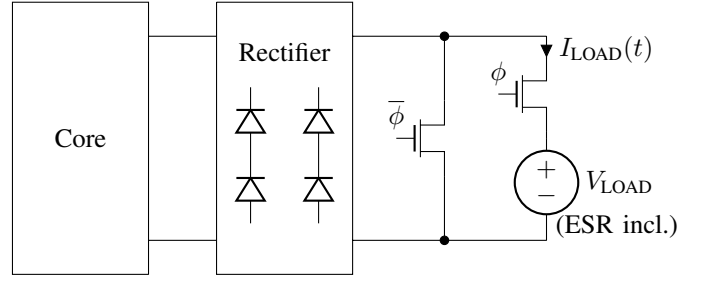


Fig. 8. Transfer window alignment circuit

B. Transfer Window Alignment (TWA)

Alternatively, it is possible to actively control the connection between the magnetic core and the load, and manipulate the starting point of the transfer window relative to the zero crossing of the primary current. This manipulation is possible because the load voltage is independent of the primary current for the case of a constant voltage load. Assuming ideal rectifiers, the duration of the transfer window is:

$$t_{SAT} = \frac{2 B_{SAT} A_{CORE} N}{V_{LOAD}} \quad (9)$$

That is, the core will be saturated if V_{LOAD} is connected to the core for t_{SAT} seconds, regardless of when the transfer window begins relative to the primary current. Given this understanding, the transfer window which permits the greatest energy harvest corresponds with a window of time when the primary current is as large as possible. We seek, then, to align the middle of the transfer window with the peak of the transformer current, and “short out” the core, reducing the voltage on the secondary winding to zero, during times outside the transfer window in order to prevent the core from developing unnecessary flux. Without a detailed nonlinear description of the magnetic core, an estimate for the average power harvest using this transfer window alignment method is,

$$P_{LOAD, avg} = V_{LOAD} \times \frac{2}{T} \int_{\frac{T}{4} - \frac{t_{SAT}}{2}}^{\frac{T}{4} + \frac{t_{SAT}}{2}} \frac{I_P}{N} \sin(\omega t) dt \quad (10)$$

$$= P_{TWA} \cdot \frac{\sin(J)}{J}$$

where

$$P_{TWA} = \frac{2 I_P \omega B_{SAT} A_{CORE}}{\pi} \quad (11)$$

$$J = \omega \frac{B_{SAT} A_{CORE} N}{V_{LOAD}} = \omega \frac{t_{SAT}}{2}$$

Since $\sin(J)/J$ has an asymptote of 1 as $J \rightarrow 0$, P_{TWA} is the maximum value of $P_{LOAD, avg}$. This indicates that we should minimize J as much as possible for higher power harvest. However, J cannot be arbitrarily small, as t_{SAT} would become proportionally small as well. If t_{SAT} becomes extremely small, subtle non-ideal effects, e.g., dynamic characteristics (early recovery) of the magnetizing inductance, dominate, and the power harvest deviates from predictions and becomes smaller. In addition, much finer time resolution is required for gate

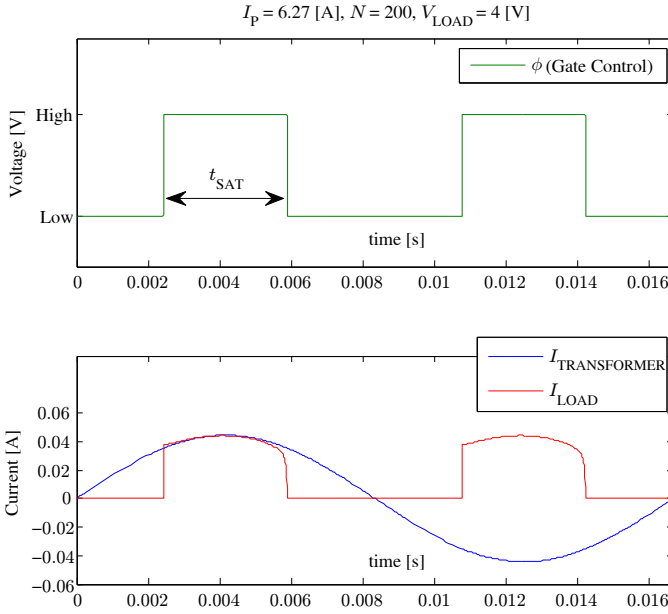


Fig. 9. Time domain waveform with the transfer window alignment

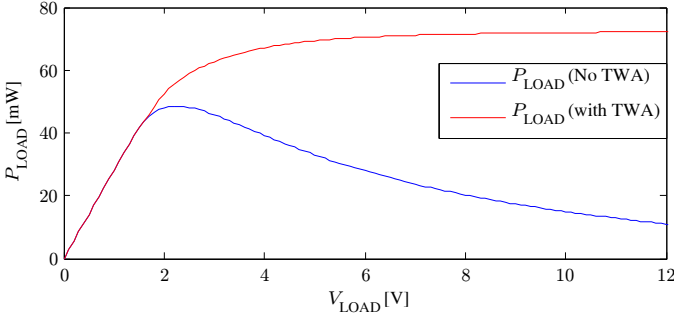


Fig. 10. Power harvest enhancement with the transfer window alignment

control. A practical rule of thumb for design is to select $t_{SAT} \geq T/10$, in which case $J \geq 0.314$, a suggestion based on our experimentation with high permeability cores.

Given a core material with known magnetic properties and size, there are essentially two parameters available to the designer, N and V_{LOAD} , for minimizing J . Decreasing N increases the secondary side current and enhances losses in the switches and diodes. The voltage V_{LOAD} cannot be arbitrarily high due to the voltage rating of the switching devices in the rectifier. Raising V_{LOAD} may also incur unnecessary losses in the digital circuits that would typically form the sensor and communication load. Therefore, N and V_{LOAD} must be carefully chosen to minimize J without incurring unnecessary losses in the rest of the harvester circuit. One aspect that can aid to loosen the design constraint is that, since minimizing J has a diminishing return on the amount of power harvest, we can actually settle at a more reasonable value of J . It may be tolerable to slightly increase J from the value for a maximum harvest in order to optimize overall system losses. For example, we might pick $J = 0.6$, providing approximately 94% of the maximally achievable power harvest, P_{TWA} , while reducing the control power and the switching loss of a diode full bridge rectifier.

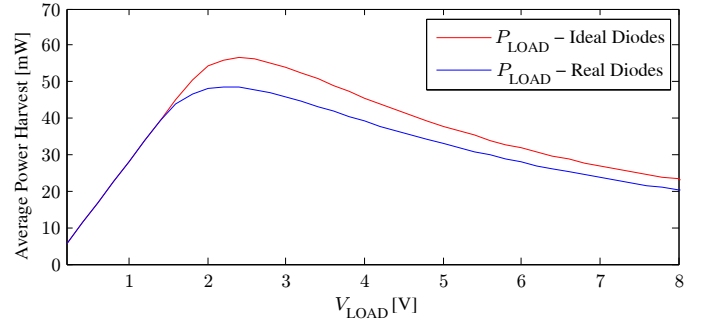


Fig. 11. Effect of real diodes in a rectifier on harvestable power

The TWA method requires only two additional switches after the rectifier, as shown in Fig. 8, and does not require any on-the-fly component change as was needed for the flux-shaping capacitor method. In Fig. 8, ϕ indicates a phase where we connect the load to the core, and $\bar{\phi}$ indicates the opposite phase. The simulation, presented in Fig. 9, clearly illustrates the shifted transfer window. Note both plots in Fig. 9 are generated with the same time reference. Using the same $I_p = 6.27A$ and $N = 200$, Fig. 10 demonstrates the enhancement of power harvest with appropriate transfer window alignment. The maximum power harvest is much higher with TWA. Nonideal diodes with a diode voltage drop of 0.19 V for the rectifier were used to generate Fig. 10. Effects of nonideal diodes will be discussed in the following section.

The TWA approach drives the core into saturation more definitively than for the FSC method. As J is minimized for enhancing the power harvest, t_{SAT} becomes shorter, which means the core goes deeper into the saturation regime.

C. Rectifier with Active Gate Control

Using either of the above methods, to extract power from the core, the switching devices in a rectifier must be operated in accordance with the polarity of the transformer current so that the current flows only from the core into the load. Diodes naturally enforce this condition. However, a rectifier implemented with diodes actually has an unavoidable diode voltage drop, V_{DIODE} . Because the core is a current-driven transformer, the load current always sees two diode voltage drops with no dead time, except for saturation where the load current is zero. Therefore, the power dissipation in these diodes must be accounted:

$$P_{SWITCH} = 2 I_{LOAD,avg} \cdot V_{DIODE} \quad (12)$$

The core sees $V_{LOAD} + 2V_{DIODE}$ instead of V_{LOAD} alone. The rectification contributes to the effectively higher core voltage, so t_{SAT} from the previous analysis is at least slightly overestimated. Figure 11 illustrates the effect of real diodes in a rectifier. In this example, we used $I_p = 6.27A$ and $N = 200$; neither the FSC method nor the TWA method is applied. The P_{LOAD} vs. V_{LOAD} response with nonideal diodes shifts to the left due to faster saturation, and is lowered by P_{SWITCH} due to diode loss. Note that P_{SWITCH} is generally different in every point along the V_{LOAD} axis, since $I_{LOAD,avg}$ is affected by the level of core saturation.

In order to minimize this loss, active rectification can be used as shown in Fig. 12, which uses transistors instead of diodes for lower on-resistance. Once the appropriate switching devices are selected for the correct current path, the cross-coupled PFET pair reduces the switching loss by one diode stage loss without any burden on gate control efforts, because the load voltage connected to the core is also powering the PFETs consistently with the selected current path. However, since a FET is a bi-directional device, it cannot block backward conduction, and automatic switching of the current paths based on the cross-coupled pair itself is not possible. That is, unless externally controlled (by diodes, for example), the PFET turns off when $|V_{GS,p}|$ becomes lower than $|V_{TH,p}|$ regardless of the direction of the transformer current. Therefore, the voltage of the rectifier output will fall until the FET is in the cut-off region. This leads to power flow from the load into the core, and significantly undermines the power harvest. For this reason, cross-coupled pairs in both top and bottom cannot be used to completely eliminate gate control. (however, if the core is a voltage-driven transformer, complete elimination of the gate control is possible by using cross-coupled pairs in both positions, as shown in [14] and [15]).

This issue can be avoided by applying gate control, ϕ_1 and ϕ_2 , to the lower NFET pair. Alternatively, we can place PFETs as a top pair with controllable gates, and NFETs as a cross-coupled pair in the bottom with naturally adjusted gate control signals. To avoid short-circuiting the output of the rectifier to ground through the FETs, we need to ensure a finite nonoverlap period between ϕ_1 and ϕ_2 . During this period, the polarity crossover of the transformer current happens, and the switching of the current paths is automatically handled by the diodes. If we denote the diode operated duration, the FET operated duration, and the on-resistance of the FET as t_{DIODE} , t_{FET} , and R_{ds-on} , respectively, the switching loss can be written as:

$$\begin{aligned}
 P_{SWITCH} = & V_{DIODE} \cdot \frac{2}{T} \int_0^{t_{DIODE}/2} I_{LOAD}(t) dt \\
 & + R_{ds-on} \cdot \frac{2}{T} \int_{t_{DIODE}/2}^{t_{DIODE}/2+t_{FET}} I_{LOAD}^2(t) dt \\
 & + V_{DIODE} \cdot \frac{2}{T} \int_{t_{DIODE}/2+t_{FET}}^{t_{DIODE}+t_{FET}} I_{LOAD}(t) dt \\
 & + R_{ds-on} \cdot \frac{2}{T} \int_0^{T/2} I_{LOAD}^2(t) dt
 \end{aligned} \quad (13)$$

where

$$t_{FET} = \min \left[t_{SAT} - \frac{t_{DIODE}}{2}, \frac{T}{2} - t_{DIODE} \right] \quad (14)$$

If we apply the proposed active gate control method to the peak point of the blue graph in Fig. 11, where $V_{DIODE} = 0.19$ V, and $I_{LOAD,avg} = 22.07$ mA, the switching loss is decreased from 8.387 mW to 0.176 mW, which is 97.9% in reduction. We assumed $t_{DIODE}/T = 5\%$ and $R_{ds-on} = 0.1 \Omega$. Compared to the power harvest with a diode rectifier providing 48.5 mW, the active gate control increases the power harvest by 16.9%.

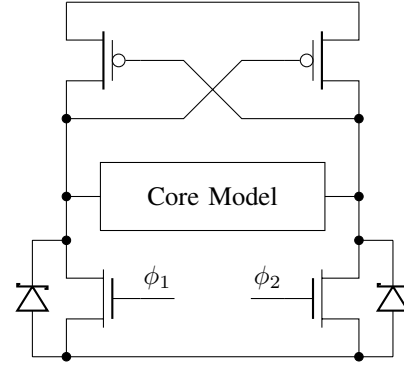


Fig. 12. Rectifier with active gate control

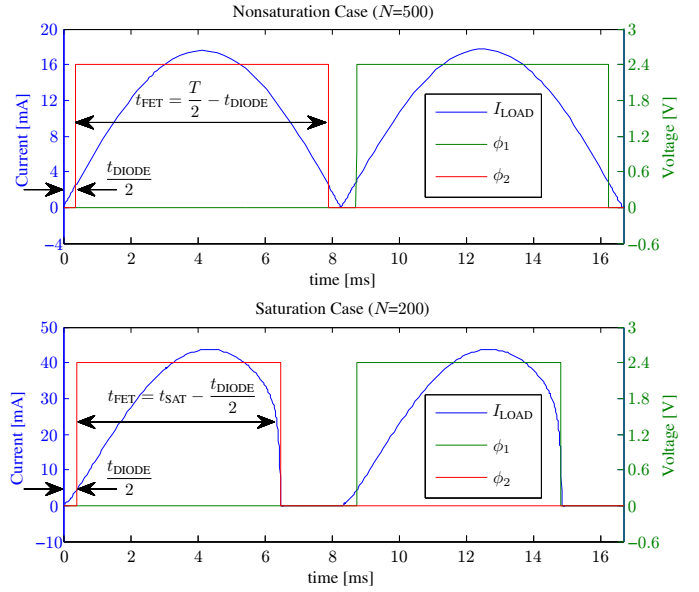


Fig. 13. ϕ_1 and ϕ_2 controls in two possible cases

Figure 13 illustrates two possible cases of ϕ_1 and ϕ_2 control based on the circuit of Fig. 12. The upper case illustrates a situation with sufficiently low output voltage that the core does not saturate during the entire cycle. The lower case exhibits saturation. In this case, the transformer current is going through the left PFET and the right NFET (ϕ_2) in the first half cycle, and then the right PFET and the left NFET (ϕ_1) in the second half cycle. When the core goes into saturation, we need to turn both NFETs off. Otherwise, one of the PFETs will be turned on due to the NFET providing a ground, and the saturated core would complete a short circuit path between the output and the ground by forcing zero voltage between two drain terminals of the turned-on transistors. Since this severely harms the power harvest, t_{FET} has a limit value of $t_{SAT} - t_{DIODE}/2$ in saturation. To incorporate this with a nonsaturating case, the min function is used in (14).

V. CONCLUSION

This paper has presented a core model for accounting for saturation behavior in magnetic energy harvesters. The model is suitable for use in circuit simulators like SPICE. Appropriate model simplifications ease computational burden,

and the model continues to show excellent accuracy across various I_p and N configurations, and on two different load types. This remains true even for cores with a large ratio of outer radius to inner radius.

Three techniques can be used to enhance the extraction of energy from a magnetic core. The first involves a flux shaping capacitor. This capacitor, in series with the core, shapes the flux accumulation of the core in a convex manner, lengthening the transfer window. The second approach uses switches to align the transfer window with the peak transformer current. By exploiting the core's indifference to the starting point of the transfer window, the load can be connected to the core when the load can receive the maximum power during the transfer time segment. The third technique uses active rectifiers to minimize losses where appropriate for the harvester application. This reduces the switching loss, and realizes the circuit environment as if we have ideal diodes with which we have done the transfer window analysis.

In practice, the harvester is likely to face one of three cases for the primary current. First is when the RMS current in the primary side is well-defined, and does not change much. In this case, a fixed flux shaping capacitor can be used reliably, eliminating control effort. Second, the primary current may exhibit substantial change over time, and a microcontroller is likely to be available as part of the sensor package powered by the harvester. In this case, the TWA method permits adaptive control of the transfer window to optimize power transfer, much like finding the maximum power point for a solar panel. Of course, if a controller cannot be deployed, a basic rectifier can be used without enhancement to harvest some power. Combinations of the three methods presented here may also be desirable in some primary current profiles.

VI. ACKNOWLEDGMENT

The authors thank the Kwanjeong Educational Foundation and the ONR Structural Acoustics Program for the support for this work, and the gifted guidance of Deborah Nalchajian.

REFERENCES

- [1] J. Moon, S. Leeb, "Analysis model for magnetic energy harvesters," *IEEE Trans. Power Electronics* (submitted)
- [2] J. Moon, J. Donnal, J. Paris, S. Leeb, "VAMPIRE: A magnetically self-powered sensor node capable of wireless transmission," *Applied Power Electronics Conference and Exposition (APEC), 2013 Twenty-Eighth Annual IEEE*, Mar. 2013.
- [3] F. Simjee and P. Chou, "Everlast: Long-life, supercapacitor-operated wireless sensor node," *Proc. 2006 International Symposium on Low Power Electronics and Design. ACM*, pp. 197-202, 2006.
- [4] P. Stanley-Marbell and D. Marculescu, "An $0.9 \times 1.2''$, low power, energy-harvesting system with custom multi-channel communication interface," *Proc. Conference on Design, automation and test in Europe. EDA Consortium*, pp. 15-20, 2007.
- [5] M. Minami, T. Morito, H. Morikawa, and T. Aoyama, "Solar biscuit: A battery-less wireless sensor network system for environmental monitoring applications," *The 2nd International Workshop on Networked Sensing Systems*, 2005.
- [6] S. Sudevalayam and P. Kulkarni, "Energy harvesting sensor nodes: survey and implications," *IEEE Commun. Surv. Tutorial*, vol. 13, no. 3, pp. 443-461, 2011.
- [7] S. Meninger, J. Mur-Miranda, R. Amirtharajah, A. Chandrakasan, and J. Lang, "Vibration-to-electric energy conversion," *IEEE Trans. Very Large Scale Integr. (VLSI) Syst.*, vol. 9, no. 1, pp. 64-76, Feb. 2001.

- [8] G. Ottman, H. Hofmann, A. Bhatt, and G. Lesieutre, "Adaptive piezoelectric energy harvesting circuit for wireless remote power supply," *IEEE Trans. Power Electron.*, vol. 17, no. 5, pp. 669-676, Sep. 2002.
- [9] A. Fowler, S. Moheimani, and S. Behrens, "A 3-DoF MEMS ultrasonic energy harvester," *2012 IEEE Sensors*, pp. 1-4, Oct. 2012.
- [10] J. Paradiso and T. Starner, "Energy scavenging for mobile and wireless electronics," *IEEE Pervasive Computing*, pp. 18-27, Jan. 2005.
- [11] I. Stark, "Thermal energy harvesting with thermo life," *IEEE Intl. Workshop on Wearable and Implantable Body Sensor Networks*, pp. 19-22, Apr. 2006.
- [12] Y. Tan and S. Panda, "Energy harvesting from hybrid indoor ambient light and thermal energy sources for enhanced performance of wireless sensor nodes," *IEEE Trans. Ind. Electron.*, vol. 58, pp. 4424-4435, Sep. 2011.
- [13] D. Brunelli, C. Moser, L. Thiele, and L. Benini, "Design of a solarharvesting circuit for batteryless embedded systems," *IEEE Trans. Circuits Syst. I, Reg. Papers*, vol. 56, no. 11, pp. 2519-2528, Nov. 2009.
- [14] A. Facen, A. Boni, "Power supply generation in CMOS passive UHF RFID tags," *Proc. 2nd Conf. Ph.D. Research Microelectronics and Electronics*, pp. 33-36, Jun. 2006.
- [15] S. Mandal and R. Sarpeshkar, "Low-power CMOS rectifier design for RFID applications," *IEEE Trans. Circuits Syst. I, Reg. Papers*, vol. 54, no. 6, pp. 1177-1188, Jun. 2007.